

# Geodesic motion in the space–time of a cosmic string

Betti Hartmann <sup>\*</sup> and Parinya Sirimachan <sup>†</sup>

School of Engineering and Science, Jacobs University Bremen, 28759 Bremen, Germany

PACS Numbers: 11.27.+d, 98.80.Cq, 04.40.Nr

## Abstract

We study the geodesic equation in the space–time of an Abelian–Higgs string and discuss the motion of massless and massive test particles. The geodesics can be classified according to the particles energy, angular momentum and linear momentum along the string axis. We observe that bound orbits of massive particles are only possible if the Higgs boson mass is smaller than the gauge boson mass, while massless particles always move on escape orbits. Moreover, neither massive nor massless particles can ever reach the string axis for non–vanishing angular momentum. We also discuss the dependence of light deflection by a cosmic string as well as the perihelion shift of bound orbits of massive particles on the ratio between Higgs and gauge boson mass and the ratio between symmetry breaking scale and Planck mass, respectively.

## 1 Introduction

Cosmic strings have gained a lot of renewed interest over the past years due to their possible connection to string theory [1]. These are topological defects [2] that could have formed in one of the numerous phase transitions in the early universe due to the Kibble mechanism. Inflationary models resulting from string theory (e.g. brane inflation) predict the formation of cosmic string networks at the end of inflation [3]. It would be very interesting to observe these objects in the universe. In recent years the detection of these objects has focused on the Cosmic Microwave background (CMB) data [4], though other observational effects such as gravitational lensing have also been discussed [5]. Here we discuss the possibility that cosmic strings might be detected due to the way that test particles move in their space–time.

Until now the geodesic motion of test particles in space–times containing cosmic strings has been mostly studied in the limit of vanishing width of the cosmic string. Since the space–time of an infinitely thin cosmic string is locally flat [2] geodesics are just straight lines. In [6] a general cosmic space–time has been studied and it has been shown that the geodesics of massless particles must move to infinity in both direction. Geodesics in cosmic string space–times have also been used to explain the motion of particles in elastic solids [7]. Furthermore, black hole space–times containing infinitely thin cosmic strings have been investigated both for static black holes [8, 9, 10, 11] as well as for rotating black holes [9, 12, 13, 14, 15]. In this case, analytic solutions to the geodesic equation in terms of elliptic functions are possible.

In this paper we are aiming at understanding particle motion in the space–time of a finite width cosmic string. The underlying field theoretical model is the  $U(1)$  Abelian–Higgs model which has string–like solutions [16]. The gravitational properties of Abelian–Higgs strings have also been studied in detail by minimally coupling the Abelian–Higgs model to gravity. Far away from the core of the string, the space–time has a deficit angle, i.e. corresponds to Minkowski space–time minus a wedge [17]. The deficit angle is in linear order proportional to the energy per unit length of the string. If the vacuum expectation value (vev) of the Higgs field is sufficiently

---

<sup>\*</sup>email: b.hartmann@jacobs-university.de

<sup>†</sup>email: p.sirimachan@jacobs-university.de

large (corresponding to very heavy strings that have formed at energies much bigger than the GUT scale), the deficit angle becomes larger than  $2\pi$ . These solutions are the so-called “supermassive strings” studied in [18] and possess a singularity at a maximal value of the radial coordinate, at which the angular part of the metric vanishes. Interestingly, it was realized only a few years ago [19, 20] that both the globally regular string solution as well as the supermassive solution have “shadow” solutions that exist for the same parameter values. The string-like solutions with deficit angle  $< 2\pi$  have a shadow solution in the form of so-called Melvin solutions, which have a different asymptotic behaviour of the metric and have higher energies than their string counterparts (and are thus very likely cosmologically not relevant). The supermassive string solutions on the other hand have shadow solutions of Kasner-type. Kasner solutions possess also a singularity at some finite radial distance, the difference is that for Kasner solutions, the  $tt$ -component of the metric vanishes at this maximal radial distance, while the angular part of the metric diverges there. Since both supermassive as well as Kasner solutions contain space-time singularities they are surely of limited interest for cosmological applications. In this paper we thus concentrate on the motion of test particles in the space-time of a gravitating cosmic string that possesses a deficit angle  $< 2\pi$ . Since the field theoretical solutions and in particular the metric functions can only be determined numerically analytic results are not possible for the geodesic equation. This is similar to the geodesic motion in the space-time of a gravitating magnetic monopole [21], where also only numerical results are possible.

Our paper is organised as follows: in Section 2, we discuss the field theoretical model that possesses string-like solutions and we also give the geodesic equation. In Section 3 we discuss our numerical results, in particular we give examples of orbits and demonstrate how the ratio between the symmetry breaking scale as well as the ratio between the Higgs and gauge boson mass influence our results. We conclude in Section 4.

## 2 The model

In the following we will first present the space-time of an Abelian-Higgs string and then give the geodesic equation that describes the motion of massless and massive test particles in the space-time of an Abelian-Higgs string.

### 2.1 The space-time of an Abelian-Higgs string

The Abelian-Higgs model is a field theoretical model with cosmic string solutions [16]. Here, we couple this model minimally to gravity. The action then reads

$$S = \int d^4x \sqrt{-g} \left( \frac{1}{16\pi G} R + \mathcal{L}_m \right) \quad (1)$$

where  $R$  is the Ricci scalar and  $G$  denotes Newton’s constant. The matter Lagrangian  $\mathcal{L}_m$  is given by

$$\mathcal{L}_m = D_\mu \phi (D^\mu \phi)^* - \frac{1}{4} F_{\mu\nu} F^{\mu\nu} - \frac{\lambda}{4} (\phi \phi^* - \eta^2)^2 \quad (2)$$

with the covariant derivative  $D_\mu \phi = \nabla_\mu \phi - ie A_\mu \phi$  and the field strength tensor  $F_{\mu\nu} = \partial_\mu A_\nu - \partial_\nu A_\mu$  of the U(1) gauge potential  $A_\mu$  with coupling constant  $e$ . The field  $\phi$  is a complex scalar field (Higgs field).

The most general, cylindrically symmetric line element invariant under boosts along the  $z$ -direction is

$$ds^2 = N^2(\rho) dt^2 - d\rho^2 - L^2(\rho) d\varphi^2 - N^2(\rho) dz^2 . \quad (3)$$

For the matter and gauge fields, we have [16]:

$$\phi(\rho, \varphi) = \eta h(\rho) e^{in\varphi} \quad , \quad A_\mu dx^\mu = \frac{1}{e} (n - P(\rho)) d\varphi , \quad (4)$$

where  $n$  is an integer indexing the vorticity of the Higgs field around the  $z$ -axis. As is apparent from the Ansatz the cosmic string possesses a magnetic field along the  $z$ -axis with [19]

$$B_z(\rho) = -\frac{1}{eL(\rho)} \frac{dP(\rho)}{d\rho} . \quad (5)$$

There are three mass scales in our model: the Higgs mass  $M_H = \sqrt{\lambda}\eta$ , the gauge boson mass  $M_W = \sqrt{2}e\eta$  as well as the Planck mass  $M_{Pl} = G^{-1/2}$ . The Bogomolny limit  $\lambda = 2e^2$  [22] corresponds to equal gauge and Higgs boson mass. The cosmic string has finite width. In fact there is a scalar core with width  $\rho_H \sim M_H^{-1}$  and a magnetic flux tube core with width  $\rho_W \sim M_W^{-1}$ . In the Bogomolny limit  $\rho_H = \rho_W$ .

We can then do the following rescaling

$$\rho \rightarrow \frac{\rho}{e\eta} \quad , \quad L \rightarrow \frac{L}{e\eta} . \quad (6)$$

such that the total Lagrangian only depends on the following dimensionless coupling constants

$$\gamma = 8\pi G\eta^2 \quad , \quad \beta = \frac{\lambda}{e^2} . \quad (7)$$

Note that  $\gamma$  is proportional to the square of the ratio of the symmetry breaking scale  $\eta$  and the Planck mass  $M_{Pl}$ , while  $\beta$  is proportional to the square of the ratio between the Higgs boson mass  $M_H$  and the gauge boson mass  $M_W$ .

Varying the action with respect to the matter fields and metric functions, we obtain a system of four non-linear differential equations. The Euler-Lagrange equations for the matter field functions read:

$$\frac{(N^2 L h')'}{N^2 L} = \frac{P^2 h}{L^2} + \frac{\beta}{2} h(h^2 - 1) \quad (8)$$

$$\frac{L}{N^2} \left( \frac{N^2 P'}{L} \right)' = 2h^2 P , \quad (9)$$

while the Einstein equations are

$$\frac{(L N N')'}{N^2 L} = \gamma \left[ \frac{(P')^2}{2L^2} - \frac{\beta}{4} (h^2 - 1)^2 \right] \quad (10)$$

and

$$\frac{(N^2 L')'}{N^2 L} = -\gamma \left[ \frac{2h^2 P^2}{L^2} + \frac{(P')^2}{2L^2} + \frac{\beta}{4} (h^2 - 1)^2 \right] . \quad (11)$$

Here and in the following the prime denotes the derivative with respect to  $\rho$ .

The set of differential equations can only be solved numerically subject to a set of boundary conditions. The requirement of regularity at the origin leads to the following boundary conditions

$$h(0) = 0 \quad , \quad P(0) = n \quad , \quad N(0) = 1 \quad , \quad N'(0) = 0 \quad , \quad L(0) = 0 \quad , \quad L'(0) = 1 \quad , \quad (12)$$

while the finiteness of the energy per unit length requires

$$h(\infty) = 1 \quad , \quad P(\infty) = 0 \quad . \quad (13)$$

In this paper we are interested in test particle motion in the space-time of a cosmic string with deficit angle  $\Delta < 2\pi$ , i.e. we do not consider supermassive strings or space-times of Melvin- or Kasner-type in this paper. The metric functions then have the following behaviour at infinity

$$N(\rho \gg 1) = c_1 \quad , \quad L(\rho \gg 1) = c_2 \rho + c_3 \quad (14)$$

where  $c_1$ ,  $c_2$  and  $c_3$  are constants that depend on  $\beta$  and  $\gamma$  [20]. We have  $c_1 = 1$  independent on  $\gamma$  and  $c_2 = 1 - 2\gamma$  in the Bogomolny limit  $\beta = 2$ .  $c_1$  and  $c_2$  both decrease for fixed  $\gamma$  and increasing  $\beta$  with  $c_1 > 1$ ,  $c_2 > 1 - 2\gamma$  for  $\beta < 2$ , and  $c_1 < 1$ ,  $c_2 < 1 - 2\gamma$  for  $\beta > 2$ . Moreover,  $c_1$  increases with  $\gamma$  for fixed  $\beta < 2$ , while  $c_1$  decreases with  $\gamma$  for fixed  $\beta > 2$ .

In the Bogomolny limit  $\beta = 2$  which corresponds to  $M_H = M_W$  we have that  $P' = L(h^2 - 1)$  [22]. Inserting this into the Einstein equation (10) and using the boundary conditions it is easy to see that in this case  $N(\rho) \equiv 1$ , i.e. the space–time is only determined by  $L(\rho)$ .

We define as inertial mass per unit length of the solution

$$\mu = \int \sqrt{-g_3} T_0^0 d\rho d\varphi \quad (15)$$

where  $g_3$  is the determinant of the 2 + 1-dimensional space-time given by  $(t, \rho, \varphi)$ . This then reads:

$$\mu = 2\pi \int_0^\infty NL \left( (h')^2 + \frac{(P')^2}{2L^2} + \frac{h^2 P^2}{L^2} + \frac{\beta}{4} (h^2 - 1)^2 \right) d\rho \quad (16)$$

In flat space–time  $\gamma = 0$  and in the Bogomolny limit  $\beta = 2$  the energy per unit length is directly proportional to the winding number  $n$  and is given by  $\mu = 2\pi n$  [22], while the general expression for  $\mu$  in flat space–time is

$$\mu = 2\pi n f(\beta) \quad (17)$$

where  $f$  is a slowly varying function of  $\beta$  which is  $f < 1$  for  $\beta < 2$ ,  $f = 1$  for  $\beta = 2$  and  $f > 1$  for  $\beta > 2$ . For  $\gamma > 0$  and fixed  $\beta$  the mass per unit length of the solution decreases with increasing  $\gamma$ .

In linear order the deficit angle  $\Delta$  of the space–time is proportional to the product of the gravitational coupling and the energy per unit length of the string  $\gamma\mu$ . Taking the non–linear effects into account  $\Delta$  is related to  $c_2$  (see (14)) by

$$\Delta = 2\pi(1 - c_2) . \quad (18)$$

Following the discussion above, the deficit angle increases when increasing  $\gamma$  and  $\Delta = 4\pi\gamma$  for  $\beta = 2$ , while  $\Delta < 4\pi\gamma$  for  $\beta < 2$  and  $\Delta > 4\pi\gamma$  for  $\beta > 2$ . Since we are only considering space–times with  $\Delta < 2\pi$  in this paper there are restrictions on the parameters  $\gamma$  and  $\beta$ . In [20] the value of  $\gamma$  at which  $\Delta = 2\pi$  has already been investigated for some particular values of  $\beta$ . We come back to this in the numerical results section.

## 2.2 The geodesic equation

We consider the geodesic equation

$$\frac{d^2 x^\mu}{d\tau^2} + \Gamma_{\rho\sigma}^\mu \frac{dx^\rho}{d\tau} \frac{dx^\sigma}{d\tau} = 0 , \quad (19)$$

where  $\Gamma_{\rho\sigma}^\mu$  denotes the Christoffel symbol given by

$$\Gamma_{\rho\sigma}^\mu = \frac{1}{2} g^{\mu\nu} (\partial_\rho g_{\sigma\nu} + \partial_\sigma g_{\rho\nu} - \partial_\nu g_{\rho\sigma}) \quad (20)$$

and  $\tau$  is an affine parameter such that for time–like geodesics  $d\tau^2 = g_{\mu\nu} dx^\mu dx^\nu$  corresponds to proper time.

The geodesic Lagrangian  $\mathcal{L}_g$  for a point particle in the space–time (3) reads

$$\mathcal{L}_g = \frac{1}{2} g_{\mu\nu} \frac{dx^\mu}{ds} \frac{dx^\nu}{ds} = \frac{1}{2} \varepsilon = \frac{1}{2} \left[ N^2 \left( \frac{dt}{d\tau} \right)^2 - \left( \frac{d\rho}{d\tau} \right)^2 - L^2 \left( \frac{d\varphi}{d\tau} \right)^2 - N^2 \left( \frac{dz}{d\tau} \right)^2 \right] , \quad (21)$$

where  $\varepsilon = 0$  for massless particles and  $\varepsilon = 1$  for massive particles, respectively.

The constants of motion are the energy  $E$ , the angular momentum of the particle that is aligned with the axis of the string (here the  $z$ -axis)  $L_z$  and the momentum  $p_z$  in  $z$ -direction

$$E := N^2 \frac{dt}{d\tau} , \quad L_z := L^2 \frac{d\varphi}{d\tau} , \quad p_z := N^2 \frac{dz}{d\tau} . \quad (22)$$

Using these constants of motion and the rescaling (6) as well as letting  $\mathcal{E} \rightarrow \mathcal{E}/(e^2\eta^2)$ ,  $p_z \rightarrow p_z/(e\eta)$ ,  $L_z \rightarrow L_z/(e^2\eta^2)$  we can rewrite (21) as follows

$$\frac{1}{2} \left( \frac{d\rho}{d\tau} \right)^2 = \mathcal{E} - V_{\text{eff}}(\rho), \quad (23)$$

where  $\mathcal{E} = (E^2 - \varepsilon)/2$  and  $V_{\text{eff}}(\rho)$  is the effective potential

$$V_{\text{eff}}(\rho) = \frac{1}{2} \left[ E^2 \left( 1 - \frac{1}{N^2} \right) + \frac{p_z^2}{N^2} + \frac{L_z^2}{L^2} \right]. \quad (24)$$

As is obvious from (23) test particle motion is only possible for  $\mathcal{E} - V_{\text{eff}}(\rho) > 0$ . The  $\rho$ -component of the geodesic equation  $\frac{d^2\rho}{d\tau^2} = -\frac{dV_{\text{eff}}}{d\rho}$  then reads

$$\frac{d^2\rho}{d\tau^2} = (p_z^2 - E^2) \frac{N'}{N^3} + L_z^2 \frac{L'}{L^3}. \quad (25)$$

For our numerical calculations, we have rewritten the components of the geodesic equation in the following way

$$d\varphi = \pm \frac{L_z d\rho}{L(\rho)^2 \left( \frac{E^2 - p_z^2}{N(\rho)^2} - \frac{L_z^2}{L(\rho)^2} - \varepsilon \right)^{1/2}}, \quad (26)$$

$$dz = \pm \frac{p_z d\rho}{N(\rho)^2 \left( \frac{E^2 - p_z^2}{N(\rho)^2} - \frac{L_z^2}{L(\rho)^2} - \varepsilon \right)^{1/2}}, \quad (27)$$

$$dt = \pm \frac{Ed\rho}{N(\rho)^2 \left( \frac{E^2 - p_z^2}{N(\rho)^2} - \frac{L_z^2}{L(\rho)^2} - \varepsilon \right)^{1/2}}. \quad (28)$$

For positive angular momentum  $L_z$  the positive and the negative sign denote outward and inward motion, respectively. The motion becomes non-planar for  $p_z \neq 0$ .

### 3 Numerical results

The equations of motion (8)-(11) can only be solved numerically. We have done this using the ordinary differential equation solver COLSYS [23]. The relative errors of the numerical integration are on the order of  $10^{-10} - 10^{-13}$ . The numerical data for the metric functions  $N$  and  $L$  then has to be interpolated. This has been done with a piecewise cubic Hermite interpolating polynomial within MATLAB. The interpolated data can then be used to find  $t(\rho)$ ,  $\varphi(\rho)$  and  $z(\rho)$  via (26)-(28). This latter integration has been done by using the recursive adaptive Simpson quadrature within MATLAB requiring an absolute error tolerance of  $10^{-8}$ .

As mentioned above we are only interested in cosmic string space-times with  $\Delta < 2\pi$  in this paper. Since  $\Delta$  depends on both  $\gamma$  and  $\beta$  there are restrictions on these parameters. These restrictions have already been investigated in [20] for some particular values of  $\beta$ . Here, we show the domain of existence of cosmic string solutions with  $\Delta < 2\pi$  in Fig.1 where we give the value of  $\gamma_{\text{max}}$ , i.e. the value of  $\gamma$  at which the deficit angle becomes equal to  $2\pi$  in dependence on  $\beta$ .

In the following we will distinguish between bound orbits and escape orbits. Note that when we talk about bound and escape orbits we are referring to the motion in the  $x$ - $y$ -plane. The particles can, of course, move along the full  $z$ -axis from  $-\infty$  to  $+\infty$  for  $p_z \neq 0$ .

Bound orbits are orbits on which test particles move from a minimal value of  $\rho$ ,  $\rho_{\text{min}} > 0$  to a maximal value of  $\rho$ ,  $\rho_{\text{max}} < \infty$  and back again. These orbits have hence two turning points with  $(d\rho/d\tau)^2 = 0$ . On escape orbits, on the other hand, particles come from  $\rho = \infty$ , reach a minimal value of  $\rho$ ,  $\rho_{\text{min}} > 0$  and move back to  $\rho = \infty$ , which means that escape orbits have only one turning point with  $(d\rho/d\tau)^2 = 0$ . Looking at (23) it is obvious that turning points are located at those  $\rho$  at which  $\mathcal{E} - V_{\text{eff}}(\rho) = 0$ .

For all our numerical calculations we have chosen  $n = 1$ .

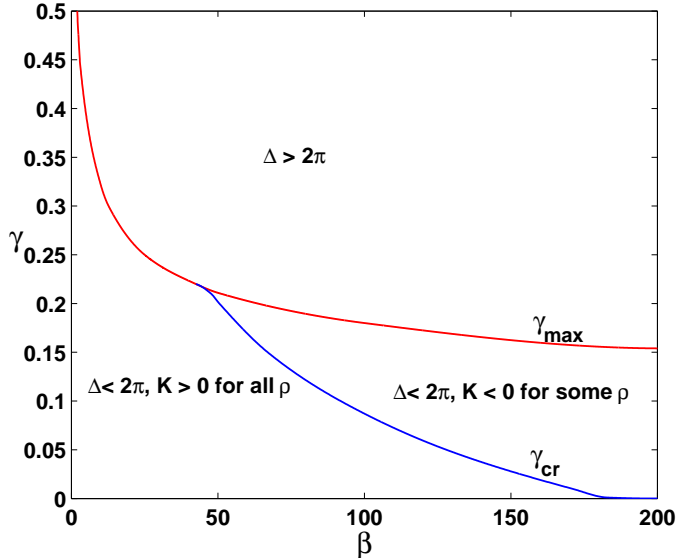


Figure 1: We show the value of  $\gamma_{\max}$ , i.e. the value of  $\gamma$  at which the deficit angle  $\Delta$  is equal to  $2\pi$  in dependence on  $\beta$ . Below this line cosmic string solutions with  $\Delta < 2\pi$  exist, while above this line the cosmic string solutions are supermassive with  $\Delta > 2\pi$  and hence possess a space–time singularity. In this paper we are only interested in solutions with  $\Delta < 2\pi$ . We also show  $\gamma_{\text{cr}}$ , i.e. the value of  $\gamma$  such that for  $\gamma > \gamma_{\text{cr}}$  the Gaussian curvature  $K$  of the 2-manifold with coordinates  $(\rho, \varphi)$  can have negative values for some  $\rho$ .

### 3.1 The effective potential

The first observation is that since  $N(\rho \rightarrow 0) \rightarrow 1$  and  $L(\rho \rightarrow 0) \rightarrow \rho$  there is always an infinite potential barrier at  $\rho \rightarrow 0$  for  $L_z \neq 0$  which means that the particles can never reach the  $z$ -axis, i.e.  $\rho = 0$ . For  $L_z = 0$  this potential barrier disappears.

Moreover, in the Bogomolny limit  $\beta = 2$  with  $N(\rho) \equiv 1$  the effective potential is monotonically decreasing from  $V_{\text{eff}}(\rho = 0) = +\infty$  to  $V_{\text{eff}}(\rho = \infty) = 0$  and  $\mathcal{E} - V_{\text{eff}}(\rho) = 0$  can only be fulfilled for one  $\rho$ . Hence in the Bogomolny limit bound orbits do not exist and test particles can only move on escape orbits. This is different for  $\beta \neq 2$  where  $N(\rho)$  is non-constant. In fact, all our numerical results indicate that bound orbits exist only for  $\beta < 2$  and for massive particles ( $\varepsilon = 1$ ). An indication that this is correct can be seen when looking at (23). Bound orbits are possible whenever  $V_{\text{eff}}$  possesses at least one extremum, i.e. there is one finite  $\rho$  for which  $dV_{\text{eff}}/d\rho = 0$ . Using the explicit form of the effective potential (24) this gives

$$\frac{dV_{\text{eff}}}{d\rho} = 0 \implies \frac{N'}{L'} = \frac{L_z^2}{E^2 - p_z^2} \frac{N^3}{L^3}. \quad (29)$$

Assuming  $N$  and  $L$  to be positive, the right-hand side of (29) is always positive. In addition  $L'$  is always positive which can be seen from (11) and the fact that  $L'(0) = 0$  and  $L'(\infty) > 0$ . Now from (11) it is easy to see that  $L' = 0$  for some finite  $0 < \rho < \infty$  is excluded. Hence, for extrema to exist we need to require that  $N' > 0$ . In fact for  $\beta < 2$  we find that  $N' > 0$ , while  $N' < 0$  for  $\beta > 2$  (see also the results in [19, 20]). Of course, the requirement that  $N' > 0$  does not guarantee that bound orbits exist (this still depends on the choice of  $\mathcal{E}$ ,  $L_z$  and  $p_z$ ), but for  $N' < 0$ , i.e.  $\beta > 2$  we can exclude the possibility of bound orbits. Our numerical results demonstrating the change of the effective potential with  $\gamma$  and  $\beta$  are shown in Fig.2. For fixed  $\gamma$  it is obvious that local extrema exist for  $\beta < 2$ , while there are no extrema for  $\beta \geq 2$ . Moreover, the potential changes only little for changing  $\beta > 2$ .

For fixed  $\beta < 2$  (here  $\beta = 1.25$ ) local extrema do exist and the value of these extrema is enhanced with increasing gravitational coupling. For fixed  $\beta > 2$  (here  $\beta = 2.5$ ) no extrema exist. While the effective potential

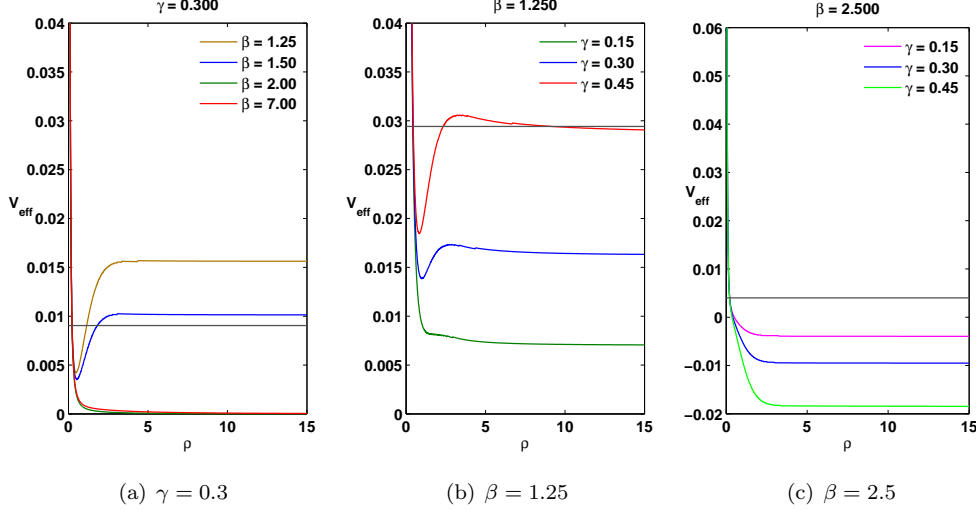


Figure 2: The effective potential for the motion of a massive test particle ( $\varepsilon = 1$ ) in the space-time of an Abelian–Higgs string is shown for fixed  $\gamma = 0.3$ ,  $E = 1.009$ ,  $p_z = 0$ ,  $L_z = 0.03$  and different values of  $\beta$  (a), fixed  $\beta = 1.25 < 2$ ,  $E = 1.029$ ,  $p_z = 0$ ,  $L_z = 0.1$  and different values of  $\gamma$  (b) and fixed  $\beta = 2.5 > 2$ ,  $E = 1.004$ ,  $p_z = 0$ ,  $L_z = 0.02$  and different values of  $\gamma$  (c). The black horizontal line represents the value of  $\mathcal{E}$ .

possesses local extrema for  $\beta < 2$  bound orbits exist only for particular choices of  $\mathcal{E}$ ,  $L_z$  and  $p_z$ . As mentioned above, our results indicate that bound orbits exist only for massive particles ( $\varepsilon = 1$ ). In order to demonstrate this, we have chosen  $\beta = 0.5$ ,  $\gamma = 0.4$ . We show the effective potential for a massive and a massless test particle in Fig.3 and Fig.4, respectively. It can be seen from Fig.3 that the potential possesses local extrema and that  $\mathcal{E}$  intersects the potential twice for sufficiently low values of  $E$  if  $\varepsilon = 1$ . This is different for the massless case. As can be seen from Fig.4, the local extrema of the effective potential disappear with decreasing  $E$  such that when  $\mathcal{E}$  is comparable to the asymptotic value of the effective potential, there are no local extrema at all. Hence, all our numerical results indicate that bound orbits for massless particles are excluded.

In the following we want to compare this result with the analytical result of [6], which states that for a general cosmic string space-time with topology  $\mathbb{R}^2 \times \Sigma$  massless test particles must move on geodesics that escape to infinity in both directions, i.e. closed geodesics are not possible. The assumption made in [6] is that  $\Sigma$  must have positive Gaussian curvature. To show that  $\Sigma$  has positive Gaussian curvature in our case, we rewrite the metric (3) for massless particles ( $ds^2 = 0$ ) moving in a plane parallel to the  $x$ - $y$ -plane as follows

$$dt^2 = \frac{1}{N^2}d\rho^2 + \frac{L^2}{N^2}d\varphi^2 = \tilde{g}_{ij}dx^i dx^j \quad , \quad i = 1, 2 \quad (30)$$

where  $\tilde{g}_{ij}$  is the so-called optical metric [24] of which the spatial projection of geodesics of massless particles, i.e. light rays are geodesics.  $\tilde{g}_{ij}$  is the metric of the above mentioned 2-manifold  $\Sigma$  and has Gaussian curvature  $K$  given by

$$\begin{aligned} K &= \frac{L'}{L}N'N - \frac{L''}{L}N^2 - (N')^2 + NN'' = \gamma N^2 (T_0^0 - T_\varphi^\varphi) + 2NN'\frac{L'}{L} - 2(N')^2 \\ &= \gamma N^2 \left( \frac{2h^2 P^2}{L^2} + \frac{(P')^2}{L^2} \right) + 2NN'\frac{L'}{L} - 2(N')^2 \end{aligned} \quad (31)$$

where in the second last equality we have used the Einstein equations (10), (11) with  $T_0^0$  the energy density and  $T_\varphi^\varphi$  the pressure in  $\varphi$ -direction. Note that (31) reduces to the relation found in [6] if we use the assumptions made in that paper, i.e.  $T_\varphi^\varphi = 0$  and  $N(\rho) \equiv 1$ .

In the BPS limit we know that  $N \equiv 1$  and the Gaussian curvature is obviously positive, away from the BPS limit one has to use the numerical solution and compute the curvature. We find that for most values of  $\beta$  and  $\gamma$  the Gaussian curvature is indeed positive and our result is in agreement with that of [6]. However, if the ratio between Higgs and gauge boson mass is sufficiently large, we find that  $K$  can become negative close to the string axis. Our results are shown in Fig.1, where we present  $\gamma_{\text{cr}}$  in dependence on  $\beta$ . For  $\gamma > \gamma_{\text{cr}}$  the Gaussian curvature  $K$  can become negative for values of  $\rho$  close to zero, while  $K$  is strictly positive for  $\gamma < \gamma_{\text{cr}}$ . Though the theorem of [6] is not applicable here, we nevertheless find that bound orbits do not exist.

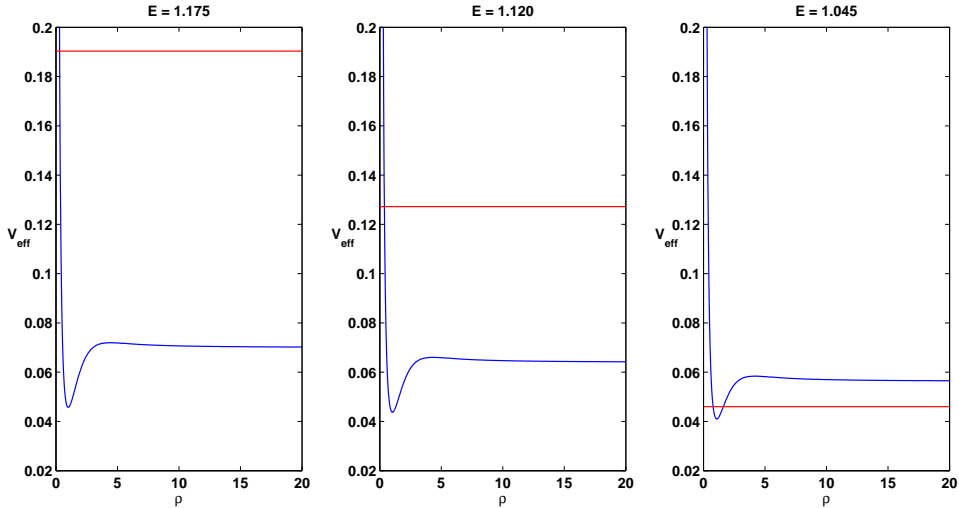


Figure 3: The effective potential for the motion of a massive test particle ( $\varepsilon = 1$ ) in the space–time of an Abelian–Higgs string with  $\beta = 0.50$  and  $\gamma = 0.40$  for different values of  $E$ . Here  $p_z = 0.100$  and  $L_z = 0.18$ . The red horizontal line represents the value of  $\mathcal{E}$ .

In Fig.5 we show how the effective potential changes with changing  $p_z$  and  $L_z$ . Increasing  $p_z$  shifts the effective potential simply to higher values which is apparent when looking at (24). Moreover, the lower the value of  $L_z$  the lower the value of the minimum of the potential. Moreover, the potential barrier at  $\rho = 0$  disappears for  $L_z = 0$ .

We have then investigated how the existence of escape and bound orbits depends on the choice of  $E$ ,  $L_z$  and  $p_z$ . Following the known discussion of orbits in the Schwarzschild case [25], we define  $\nu := L_z^2$  and  $\mu := E^2$ . In Fig.6(a) we show the  $\mu$ – $\nu$ –plane of a massive test particle for  $\beta = 0.5$ ,  $\gamma = 0.4$  and  $p_z = 0$  and indicate for which values of  $\mu$  and  $\nu$  bound orbits exist. This is only possible in regions *M2* and *M3*. The corresponding effective potential  $V_{\text{eff}}$  for regions *M1*–*M4* is shown in Fig.7. In region *M1* the effective potential  $V_{\text{eff}}$  is always larger than  $\mathcal{E}$ , so no particle motion is possible. In region *M2* the potential has a local minimum and  $\mathcal{E}$  intersects  $V_{\text{eff}}$  twice. The intersection points correspond to the minimal and maximal radius of a bound orbit. In region *M3* the potential has a local minimum and a local maximum and  $\mathcal{E}$  intersects  $V_{\text{eff}}$  three times. The two intersection points at smaller  $\rho$  correspond to the minimal and maximal radius of a bound orbit, while the intersection point at larger  $\rho$  corresponds to the minimal radius of an escape orbit. Finally, in region *M4*  $\mathcal{E}$  intersects  $V_{\text{eff}}$  once. This intersection point corresponds to the minimal radius of an escape orbit. As already mentioned the form of the effective potential will change with  $\gamma$  and  $\beta$ . This leads then to a change of the  $\mu$ – $\nu$ –plane which is indicated in Fig.6(b)–(e), where we demonstrate how the regions *M1*–*M4* change when changing either  $\gamma$  or  $\beta$ . For fixed  $\gamma$  the regions *M2* and *M3* in which bound orbits exist get smaller when increasing  $\beta$  and in fact – as stated above – disappear completely for  $\beta \geq 2$ . This is seen in Fig.6(b)–(c). Moreover, for fixed  $\beta < 2$  the regions *M2* and *M3* get bigger when increasing the gravitational coupling  $\gamma$ . This is shown in Fig.6(d)–(e).

Note that our results for  $p_z \neq 0$  are qualitatively similar, this is why we don't discuss them in detail here.



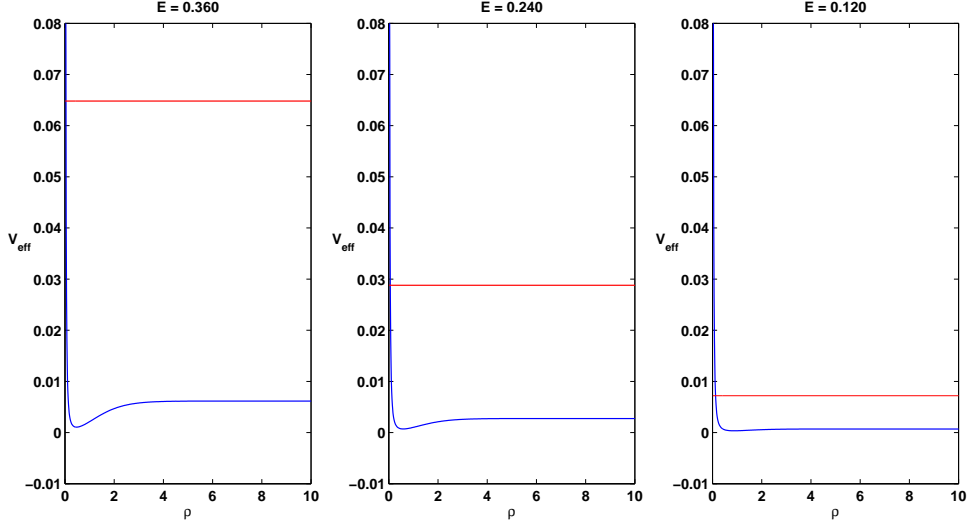


Figure 4: The effective potential for the motion of a massless test particle ( $\varepsilon = 0$ ) in the space-time of an Abelian-Higgs string with  $\beta = 0.50$  and  $\gamma = 0.40$  for different values of  $E$ . Here  $p_z = 0.100$  and  $L_z = 0.015$ . The red horizontal line represents the value of  $\mathcal{E}$ .

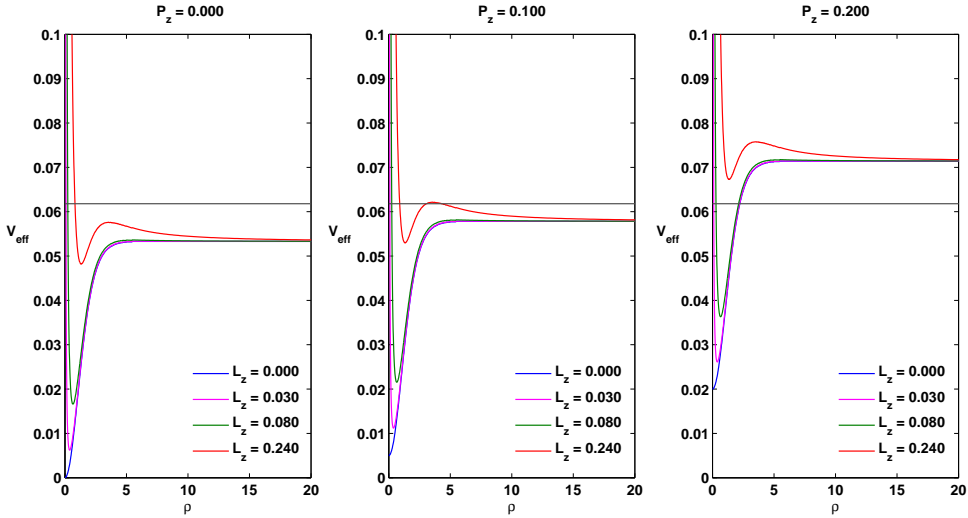
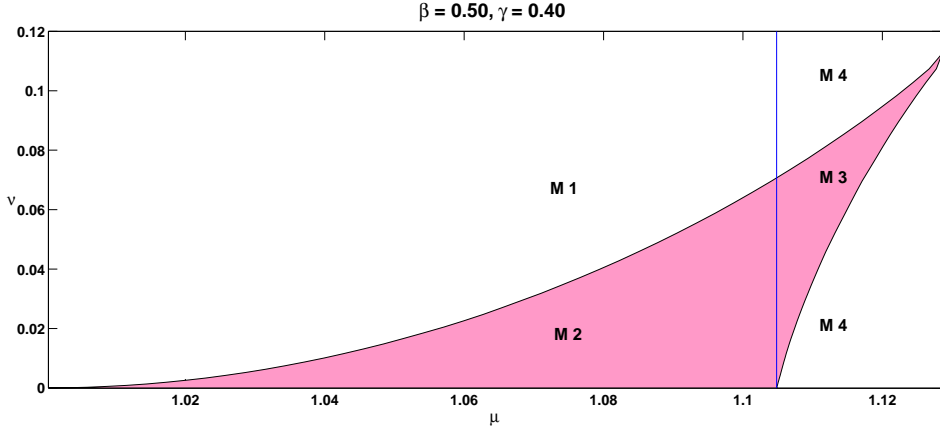
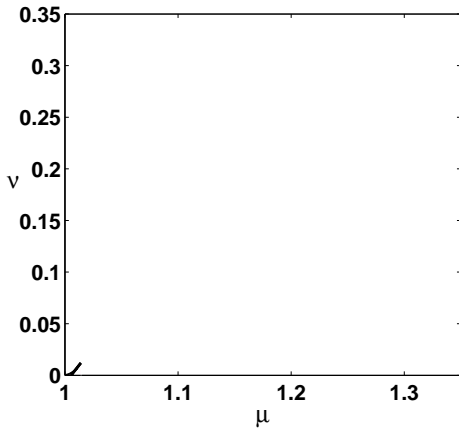


Figure 5: The effective potential for the motion of a massive test particle ( $\varepsilon = 1$ ) in the space-time of an Abelian-Higgs string with  $\beta = 0.50$  and  $\gamma = 0.40$  for different values of  $p_z$  and  $L_z$ . Here  $E = 1.060$  and  $L_z = 0.015$ . The black horizontal line represents the value of  $\mathcal{E}$ .

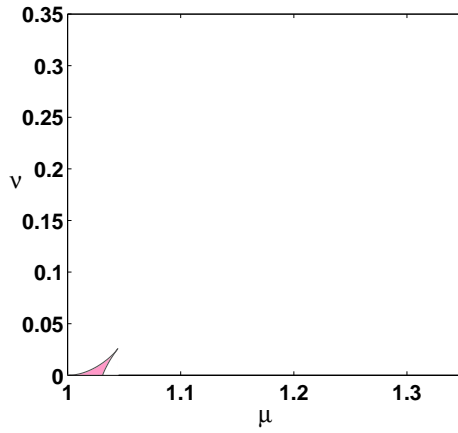
The main difference between  $p_z = 0$  and  $p_z \neq 0$  is that the particles move on 3-dimensional orbits in the latter case, while their motion is restricted to the  $x$ - $y$ -plane in the former.



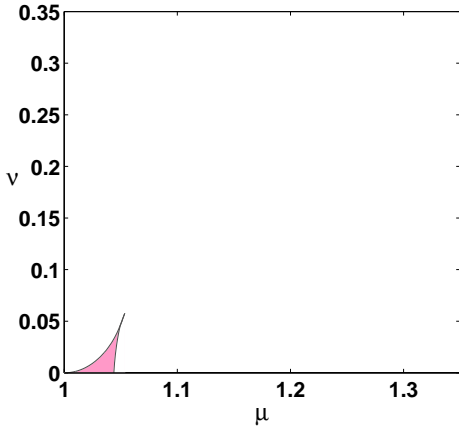
(a)  $\mu$ - $\nu$ -plane for  $\beta = 0.5$  and  $\gamma = 0.4$



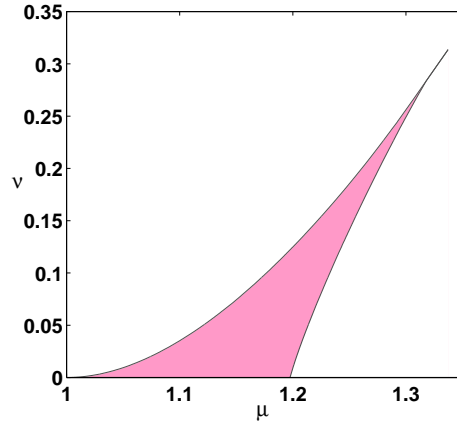
(b)  $\beta = 1.9, \gamma = 0.4$



(c)  $\beta = 1.5, \gamma = 0.4$



(d)  $\beta = 0.5, \gamma = 0.2$



(e)  $\beta = 0.5, \gamma = 0.6$

Figure 6: (a): The different regions in the  $\mu$ - $\nu$ -plane for massive test particles ( $\varepsilon = 1$ ) with  $p_z = 0$ . Bound orbits are possible in regions M2 and M3, while in M1 and M4 only escape orbits exist (see also Fig.7 for more details). The blue vertical line indicates the value of the energy at which the transition from region M3 to region M2 takes place. (b)-(e): The change of the regions M1-M4 when changing the gravitational coupling  $\gamma$  and the Higgs to gauge boson mass ratio  $\beta$ , respectively. Note that for  $\beta \geq 2$  no bound orbits exist.

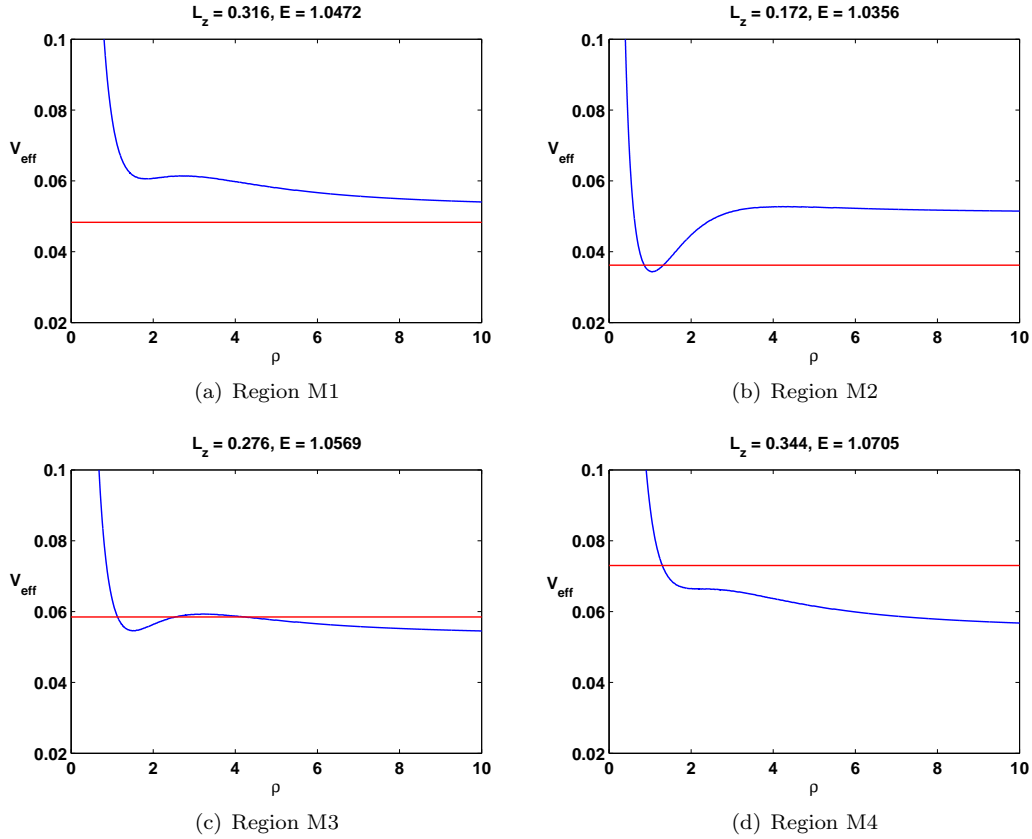


Figure 7: The effective potential  $V_{\text{eff}}(\rho)$  (blue) as well as  $(E^2 - \varepsilon)/2$  (red) are given for the different regions M1-M4 of the  $\mu$ - $\nu$ -plot (see also Fig.6). Note that for particle motion to be possible we need to require  $(E^2 - \varepsilon)/2 > V_{\text{eff}}(\rho)$ . Hence in M2 there is a bound orbit, in M3 a bound and an escape orbit, while in M4 there is an escape orbit.

## 3.2 Examples of geodesics

### 3.2.1 Massive particles $\varepsilon = 1$

In Fig.8-11 we show how bound and escape orbits of massive test particles ( $\varepsilon = 1$ ) change when changing  $\gamma$  and  $\beta$ , respectively. In order to understand how the test particle moves we also indicate the radius of the scalar core (red) and of the magnetic flux tube core (blue). Since we measure the distance  $\rho$  in units of  $M_W/\sqrt{2}$  the scalar core radius is given by  $\rho_H \sim 1/\sqrt{\beta}$  and the magnetic flux tube core is given by  $\rho_W \sim 1/\sqrt{2}$ .

From Fig.8 it is evident that the maximal radius of a bound orbit decreases strongly with increasing  $\gamma$ . While it is much larger than  $\rho_H$  for  $\gamma = 0.36$ , it becomes comparable to  $\rho_H$  for  $\gamma = 0.42$  and even smaller than  $\rho_H$  for  $\gamma = 0.48$ . This is related to the increased curvature of space–time for increasing  $\gamma$ . Moreover, the minimal radius of the escape orbit is always inside the magnetic flux tube core. Hence, the particle does not only move in the exterior (vacuum) region of the cosmic string, but can enter into the scalar and flux tube cores.

The change of a bound orbit with  $\beta$  is shown in Fig.9. The maximal radius of the bound orbit increases with increasing  $\beta$ , while the radius of the scalar core  $\rho_H$  decreases at the same time. This leads to the observation that for small  $\beta$  the particle moves basically only inside the scalar core, while for increasing  $\beta$  it moves further and further away from the cosmic string.

In Fig.10 we show how an escape orbit changes when changing the gravitational coupling  $\gamma$ . For  $\gamma = 0.15$  and  $\gamma = 0.3$  the particle arrives from infinity, gets deflected by the cosmic string and moves again to infinity. The larger  $\gamma$  the bigger is the change in the direction of the motion of the particle. This is not surprising since the deficit angle  $\Delta$  increases with increasing  $\gamma$ . For  $\gamma = 0.45$  we observe a new phenomenon. The particle arrives from infinity, encircles the cosmic string and then moves again to infinity. This is new as compared to a space–time of an infinitely thin string. However, this type of encirclement has already been observed in the space–time of a Schwarzschild black hole and Kerr black hole, respectively pierced by an infinitely thin cosmic string for sufficiently large deficit angle [11, 15]. Comparing these results with those given in Fig.11 we observe that the encirclement disappears when increasing  $\beta$ . While it is still present for  $\beta = 0.5$ , it has disappeared for  $\beta = 2$  and  $\beta = 5.3$ .

### 3.2.2 Massless particles $\varepsilon = 0$

It seems that massless particles can only move on escape orbits, i.e. bound orbits as the ones shown for massive particles are not possible. We show the change of an escape orbit with the gravitational coupling  $\gamma$  in Fig.12. For sufficiently large  $\gamma$  we observe that the massless test particle encircles the cosmic string before moving again to infinity. This is completely new as compared to the space–time of an infinitely thin cosmic string. The change of the orbit with  $\beta$  is qualitatively similar to that of a massive particle. This is why we don't present it here.

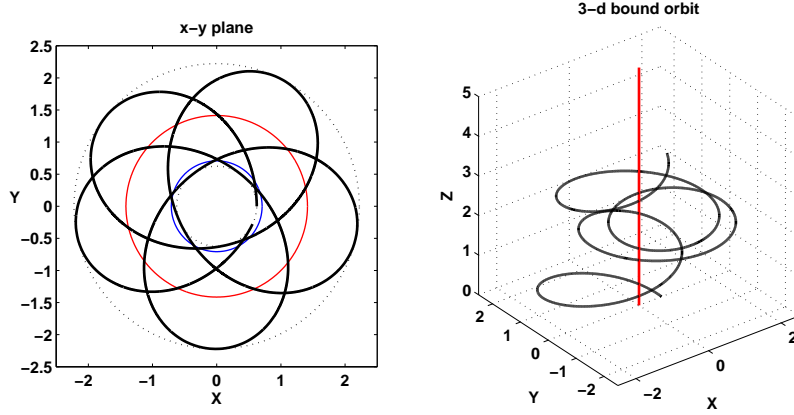
## 3.3 Observables

### 3.3.1 Perihelion shift

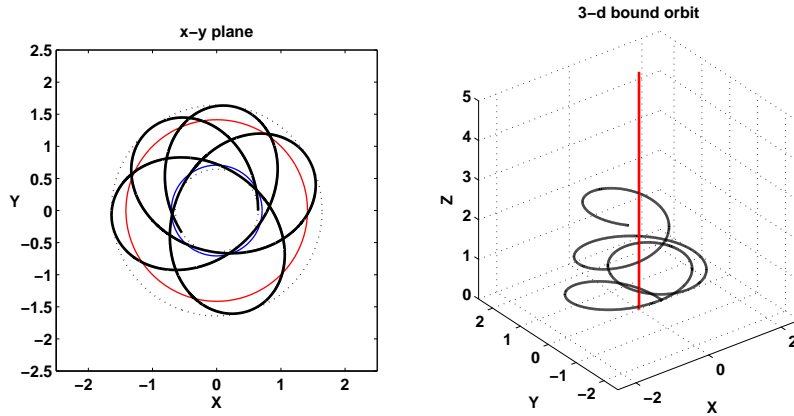
We can calculate the perihelion shift of a planar ( $p_z = 0$ ) bound orbit of a massive test particle ( $\varepsilon = 1$ ) by using (26). The perihelion shift then reads

$$\delta\varphi = 2 \int_{\rho_{\min}}^{\rho_{\max}} \frac{L_z d\rho}{L(\rho)^2 \left( \frac{E^2 - p_z^2}{N(\rho)^2} - \frac{L_z^2}{L(\rho)^2} - 1 \right)^{1/2}} - 2\pi, \quad (32)$$

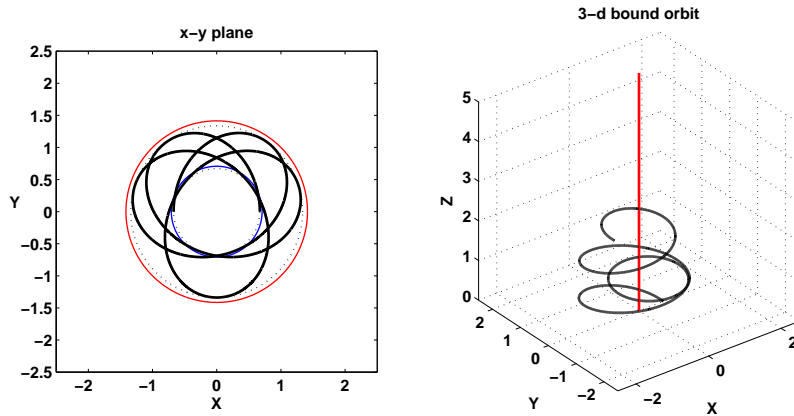
where  $\rho_{\min}$  and  $\rho_{\max}$  are the minimal and maximal radius of the bound orbit. Our results for a particle with  $E = 1.03$ ,  $L_z = 0.1$  and  $p_z = 0$  are shown in Fig.13, where the value of  $\delta\varphi$  is given in dependence on the gravitational coupling  $\gamma$  for different values of  $\beta$ . For this particular case, the perihelion shift is negative which means that the particle moves from  $\rho_{\min}$  to  $\rho_{\max}$  and back to  $\rho_{\min}$  under an angle of less than  $2\pi$ . Though in most space–times the perihelion shift is positive it is not too surprising that it can become negative in our case since the space–time is conical. Typically, the perihelion shift is negative for  $\mathcal{E}$  small, i.e. small values of the energy, while it becomes positive for larger values of  $\mathcal{E}$ .



(a)  $\gamma = 0.36$

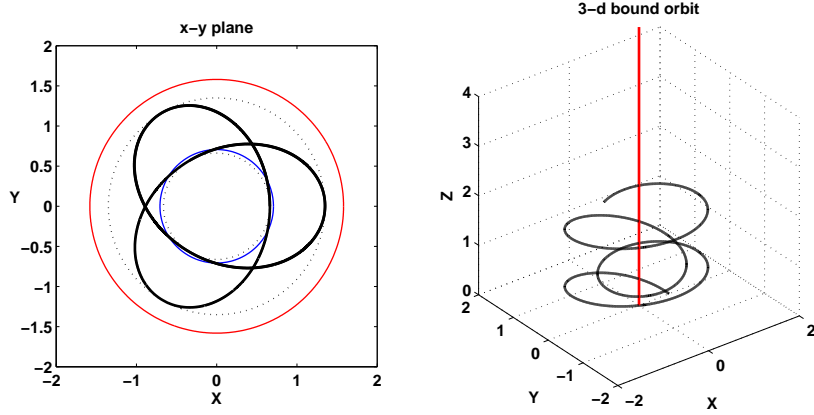


(b)  $\gamma = 0.42$

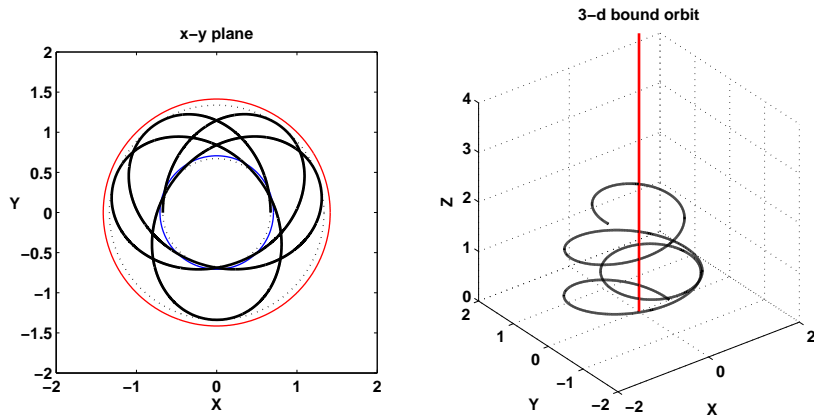


(c)  $\gamma = 0.48$

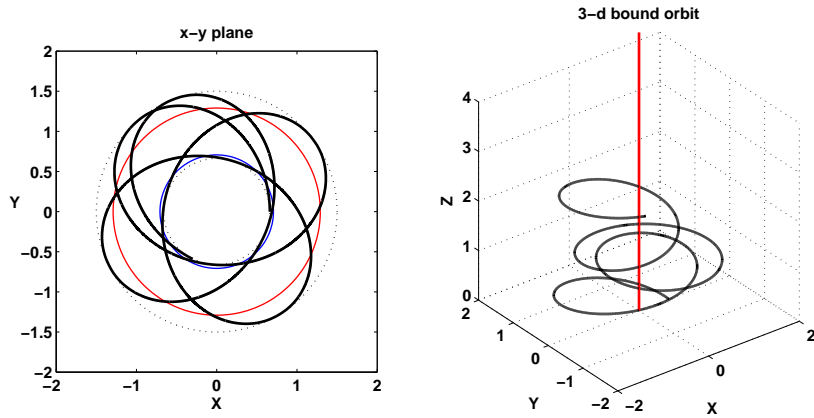
Figure 8: The change of the bound orbit of a massive test particle ( $\varepsilon = 1$ ) with  $E = 1.083$ ,  $L_z^2 = 0.025$  and  $p_z = 0.02$  due to the change of the gravitational coupling  $\gamma$ . Here, we have chosen  $\beta = 0.5$ . The red and blue circle indicates the scalar field core and the magnetic flux tube core of the Abelian-Higgs string, respectively. The dotted lines indicate the minimal and maximal  $\rho$  of the bound orbit. In the 3-dimensional plots the red line indicates the string axis.



(a)  $\beta = 0.40$

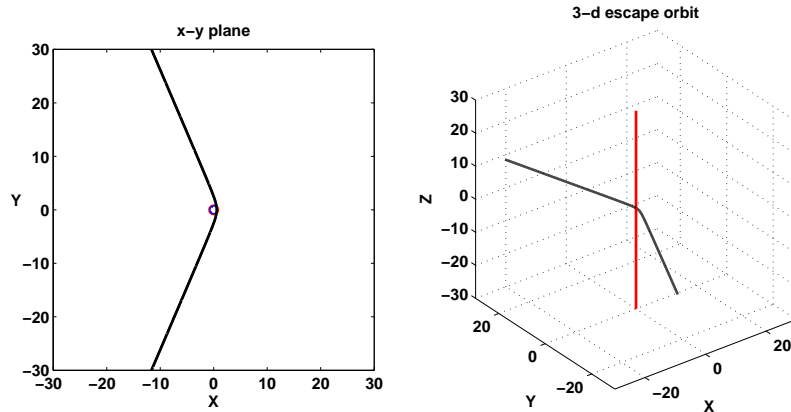


(b)  $\beta = 0.50$

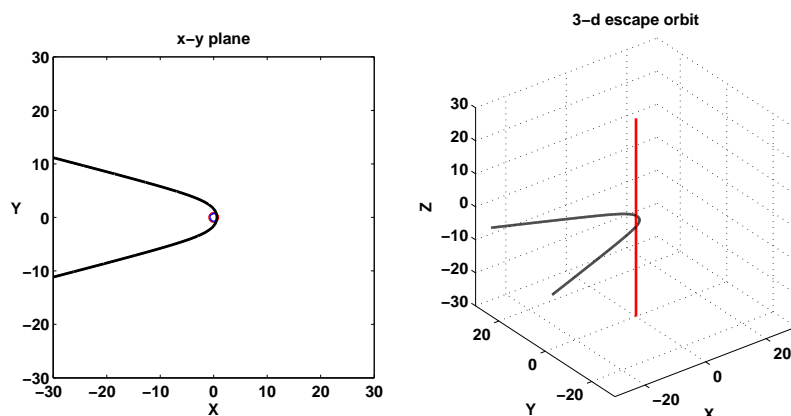


(c)  $\beta = 0.60$

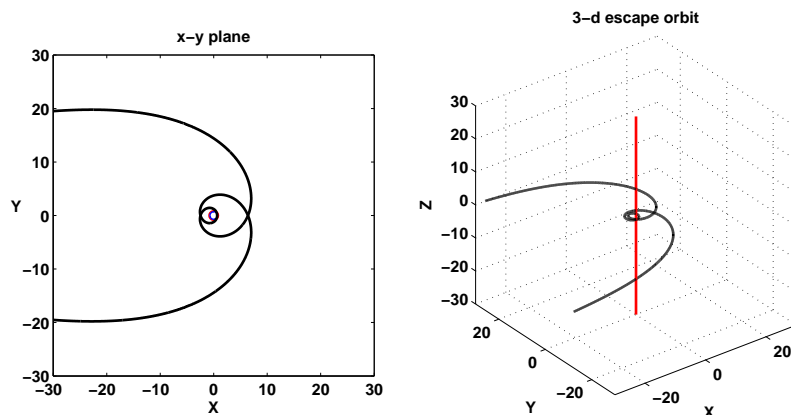
Figure 9: The change of the bound orbit of a massive test particle ( $\varepsilon = 1$ ) with  $E = 1.083$ ,  $L_z^2 = 0.025$  and  $p_z = 0.0205$  due to the change of the ratio between Higgs and gauge boson mass  $\beta$ . Here, we have chosen  $\gamma = 0.48$ . The red and blue circle indicates the scalar field core and the magnetic flux tube core of the Abelian-Higgs string, respectively. The dotted lines indicate the minimal and maximal  $\rho$  of the bound orbit. In the 3-dimensional plots the red line indicates the string axis.



(a)  $\gamma = 0.15$

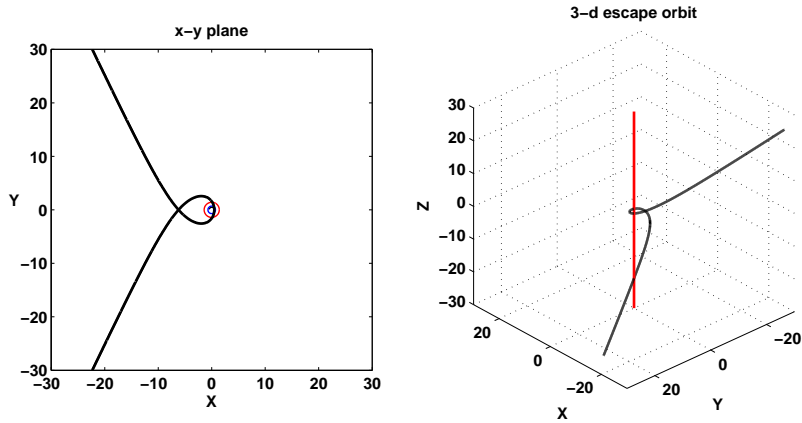


(b)  $\gamma = 0.30$

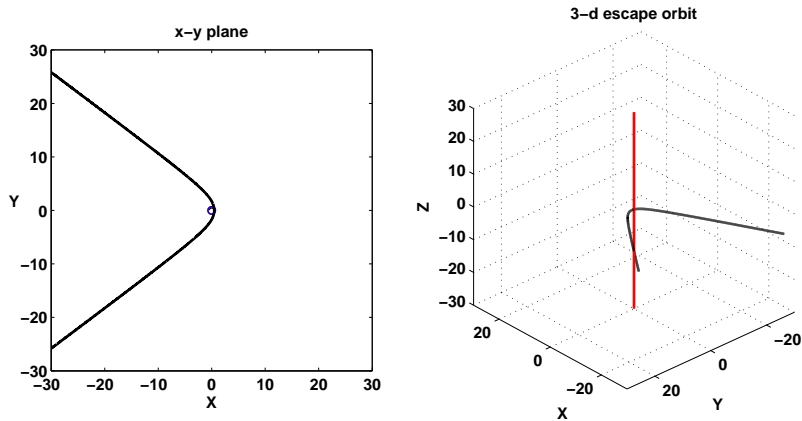


(c)  $\gamma = 0.45$

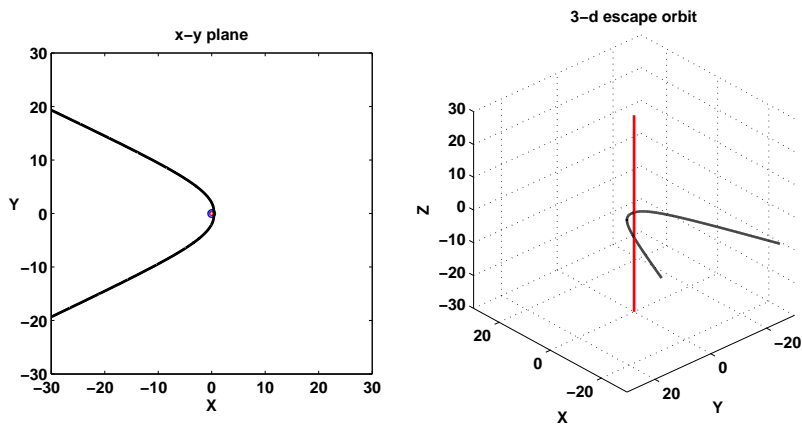
Figure 10: The change of the escape orbit of a massive test particle ( $\varepsilon = 1$ ) with  $E = 1.034$ ,  $L_z^2 = 0.02$  and  $p_z = 0.002$  due to the change of the gravitational coupling  $\gamma$ . Here, we have chosen  $\beta = 1.25$ . The red and blue circle indicates the scalar field core and the magnetic flux tube core of the Abelian–Higgs string, respectively. In the 3–dimensional plots the red line indicates the string axis.



(a)  $\beta = 0.50$



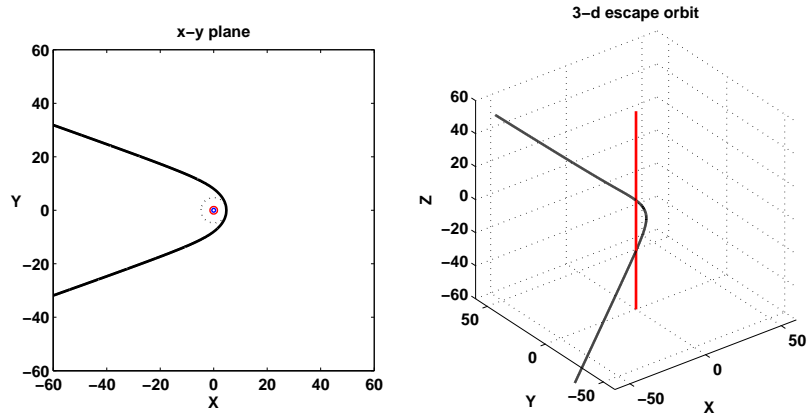
(b)  $\beta = 2.00$



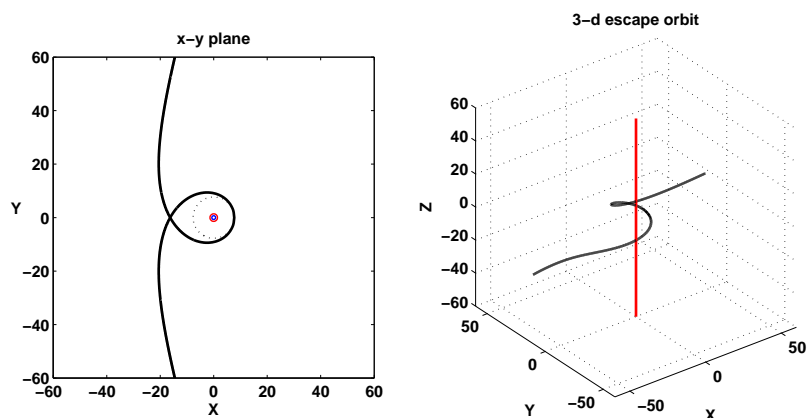
(c)  $\beta = 5.30$

Figure 11: The change of the escape orbit of a massive test particle ( $\varepsilon = 1$ ) with  $E = 1.037$ ,  $L_z^2 = 0.015$  and  $p_z = 0.03$  due to the change of the ratio between Higgs and gauge boson mass  $\beta$ . Here, we have chosen  $\gamma = 0.3$ . The red and blue circle indicates the scalar field core and the magnetic flux tube core of the Abelian-Higgs string, respectively. In the 3-dimensional plots the red line indicates the string axis.

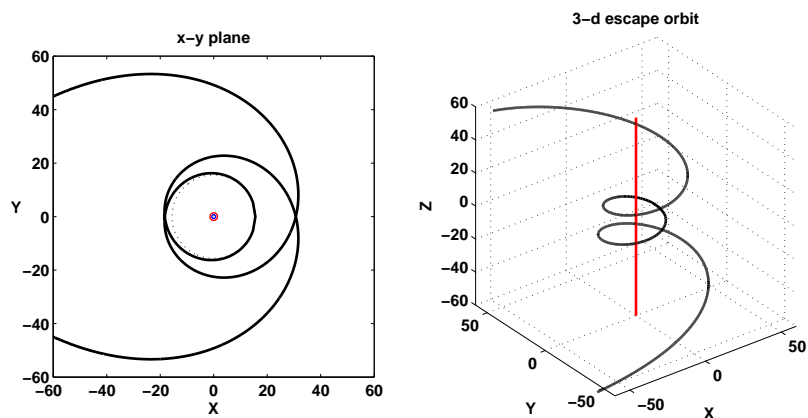




(a)  $\gamma = 0.30$



(b)  $\gamma = 0.48$



(c)  $\gamma = 0.61$

Figure 12: The change of the escape orbit of a massless test particle ( $\varepsilon = 0$ ) with  $E = 0.075$ ,  $L_z^2 = 0.03$  and  $p_z = 0.05$  due to the change of the gravitational coupling  $\gamma$ . Here, we have chosen  $\beta = 0.5$ . The red and blue circle indicates the scalar field core and the magnetic flux tube core of the Abelian–Higgs string, respectively. In the 3–dimensional plots the red line indicates the string axis.

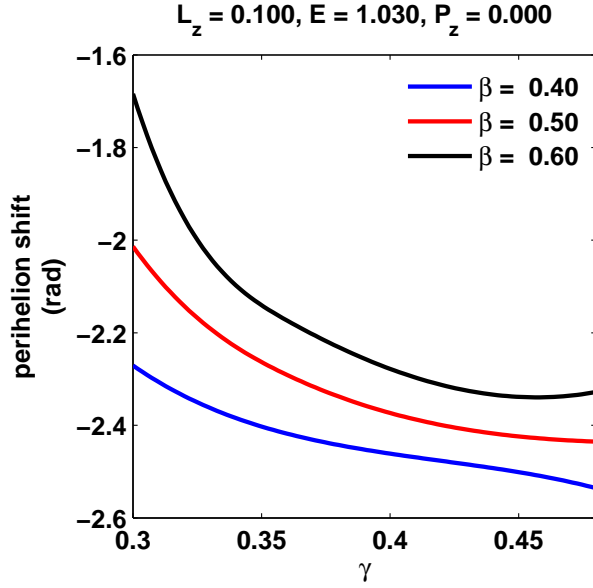


Figure 13: The dependence of the perihelion shift  $\delta\varphi$  on the gravitational coupling  $\gamma$  for three different ratios  $\beta$  of the Higgs to gauge boson mass. Here, we have chosen  $\varepsilon = 1$ ,  $L_z = 0.1$ ,  $E = 1.03$  and  $p_z = 0$ .

We observe that the value of the perihelion shift decreases for increasing  $\gamma$ . Moreover, increasing the ratio  $\beta$  between Higgs and gauge boson mass increases the value of the perihelion shift.

### 3.3.2 Light deflection

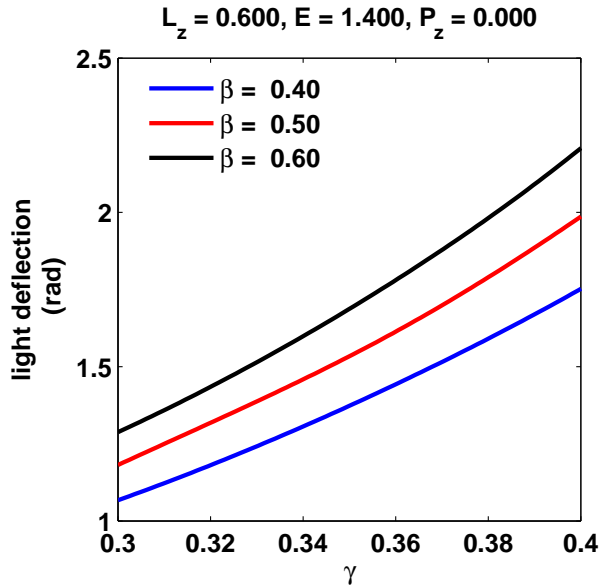


Figure 14: The dependence of the light deflection  $\widetilde{\delta\varphi}$  on the gravitational coupling  $\gamma$  for three different ratios  $\beta$  of the Higgs to gauge boson mass. Here, we have chosen  $\varepsilon = 0$ ,  $L_z = 0.6$ ,  $E = 1.4$  and  $p_z = 0$ .

The deflection of light by a cosmic string can be calculated by using (26) for a planar ( $p_z = 0$ ) escape orbit of a massless test particle ( $\varepsilon = 0$ ). The light deflection then reads

$$\widetilde{\delta\varphi} = 2 \int_{\rho_{\min}}^{\infty} \frac{L_z d\rho}{L(\rho)^2 \left( \frac{E^2 - p_z^2}{N(\rho)^2} - \frac{L_z^2}{L(\rho)^2} \right)^{1/2}} - \pi, \quad (33)$$

where  $\rho_{\min}$  is the minimal radius of the orbit.

Our numerical results are shown in Fig.14, where we give the value of  $\widetilde{\delta\varphi}$  in dependence on the gravitational coupling  $\gamma$  for three different values of  $\beta$ . Apparently, light deflection becomes stronger when increasing  $\gamma$  which results from the increase of the deficit angle. Moreover, increasing the ratio between Higgs and gauge boson mass increases the light deflection.

## 4 Conclusions

In this paper, we have studied the geodesic motion of massive and massless test particles in the space–time of an Abelian–Higgs string. We find that the existence of bound orbits, i.e. orbits on which a particle moves between a finite maximal and finite minimal radius depends crucially on the choice of the ratio between the symmetry breaking scale and the Planck mass and the choice of the ratio between the Higgs and gauge boson mass. In this paper, we have only considered the case of small symmetry breaking scale (in comparison to the Planck mass), i.e. we have only taken space-times with deficit angle smaller than  $2\pi$  into account. Moreover, we have not studied Melvin–type space-times which we believe are physically not relevant from a astrophysical/cosmological point of view.

We observe that bound orbits are only possible if the test particle is massive and if the Higgs boson mass is smaller than the gauge boson mass or in other words if the magnetic flux tube core lies inside the scalar core of the cosmic string. Increasing either the ratio between the symmetry breaking scale and the Planck mass or the ratio between the Higgs and gauge boson mass the particles move closer and closer around the string core. In fact, they move inside both the scalar and flux tube core and are not restricted to the movement inside the vacuum region outside both cores. For massless particles, which can only move on escape orbits, we observe a new phenomenon as compared to the space–time of an infinitely thin cosmic string: the particles can encircle the string before moving again to infinity.

The perihelion shift of bound orbits of massive particles can be either negative or positive depending on the particle’s energy and decreases with increasing ratio between symmetry breaking scale and Planck mass. Moreover, it increases with increasing Higgs to gauge boson mass ratio. The light deflection by a cosmic string increases with both the ratio between symmetry breaking scale and Planck mass and the ratio between Higgs and gauge boson mass. Since one of the possible detections of cosmic strings would be by light deflection (i.e. gravitational lensing) our results can be used to compare possible observational data to make predictions about the symmetry breaking scale at which the cosmic string formed as well as about the ratio between the corresponding Higgs and gauge boson mass of the underlying field theory.

It would also be interesting to study geodesic motion in the space–time of a semilocal string [26, 27, 28], which is a solution of the electroweak model with gauge group  $SU(2) \times U(1)$  in the limit where the Weinberg angle  $\theta_W = \pi/2$ . Moreover, field theoretical models describing so–called  $p$ – $q$ –strings have been studied recently [29, 30].  $p$ – $q$ –strings are supersymmetric bound states of  $F$ – and  $D$ –strings and provide one of the examples of strings that might have formed in inflationary models resulting from string theory. Understanding how test particles move in the space–time of these strings would provide a further possibility to detect them.

**Acknowledgments** We thank V. Kagramanova for discussions in the early stages of this project. The work of PS was supported by DFG grant HA-4426/5-1. We are grateful to G. Gibbons for bringing [6] to our attention.

## References

- [1] see e.g. J. Polchinski, *Introduction to cosmic F- and D-strings*, hep-th/0412244 and references therein.
- [2] A. Vilenkin and P. Shellard, *Cosmic strings and other topological defects*, Cambridge University Press (1994).
- [3] M. Majumdar and A. C. Davis, JHEP **0203** (2002) 056 [arXiv:hep-th/0202148]. S. Sarangi and S. H. H. Tye, Phys. Lett. B **536**, 185 (2002) [arXiv:hep-th/0204074].
- [4] N. Bevis, M. Hindmarsh, M. Kunz and J. Urrestilla, Phys. Rev. Lett. **100**, 021301 (2008) [arXiv:astro-ph/0702223]; Phys. Rev. D **75**, 065015 (2007) [arXiv:astro-ph/0605018]; for a recent review see C. Ringeval, *Cosmic strings and their induced non-Gaussianities in the cosmic microwave background*, arxiv: 1005.4842 (astro-ph).
- [5] see e.g. M. Yu. Khlopov, *Cosmoparticle physics*, World Scientific (1999) and references therein.
- [6] G. W. Gibbons, Phys. Lett. B **308**, 237 (1993).
- [7] A. de Padua, F. Parisio-Filho and F. Moraes, Phys. Lett. A **238** (1998) 153.
- [8] A. N. Aliev and D. V. Galtsov, Sov. Astron. Lett. **14**, 48 (1988).
- [9] D. V. Galtsov and E. Masar, Class. Quant. Grav. **6**, 1313 (1989).
- [10] S. Chakraborty and L. Biswas, Class. Quant. Grav. **13**, 2153 (1996).
- [11] E. Hackmann, B. Hartmann, C. Laemmerzahl and P. Sirimachan, Phys. Rev. D **81**, 064016 (2010) [arXiv:0912.2327 [gr-qc]].
- [12] N. Ozdemir, Class. Quant. Grav. **20** 4409 (2003).
- [13] F. Ozdemir, N. Ozdemir and B. T. Kaynak, Int. J. Mod. Phys. A **19** 1549 (2004).
- [14] S. G. Fernandes, G. De A. Marques and V. B. Bezerra, Class. Quant. Grav. **23** 7063 (2006).
- [15] E. Hackmann, B. Hartmann, C. Lämmerzahl and P. Sirimachan, *Test particle motion in the space-time of a Kerr black hole pierced by a cosmic string*, arXiv:1006.1761 [gr-qc].
- [16] H. B. Nielsen and P. Olesen, Nucl. Phys. B **61**, 45 (1973).
- [17] D. Garfinkle, Phys. Rev. D **32**, 1323 (1985).
- [18] P. Laguna and D. Garfinkle, Phys. Rev. D **40**, 1011 (1989); M. E. Ortiz, Phys. Rev. D **43**, 2521 (1991).
- [19] M. Christensen, A. L. Larsen and Y. Verbin, Phys. Rev. D **60**, 125012 (1999) [arXiv:gr-qc/9904049].
- [20] Y. Brihaye and M. Lubo, Phys. Rev. D **62**, 085004 (2000) [arXiv:hep-th/0004043].
- [21] V. Kagramanova, J. Kunz and C. Lammerzahl, Gen. Rel. Grav. **40** (2008) 1249 [arXiv:0708.1747 [gr-qc]].
- [22] E. B. Bogomolny, Sov. J. Nucl. Phys. **24** (1976) 449 [Yad. Fiz. **24** (1976) 861].
- [23] U. Ascher, J. Christiansen and R. Russell, Math. of Comp. **33**, 659 (1979); ACM Trans. **7**, 209 (1981).
- [24] M. A. Abramowicz, B. Carter and J. P. Lasota, Gen. Rel. Grav. **20**, 1173 (1988).
- [25] Y. Hagihara, *Theory of relativistic trajectories in a gravitational field of Schwarzschild*, Japan. J. Astron. Geophys. **8**, 67 (1931).
- [26] T. Vachaspati and A. Achucarro, Phys. Rev. D **44**, 3067 (1991); Phys. Rept. **327**, 347 (2000).
- [27] M. Hindmarsh, Phys. Rev. Lett. **68**, 1263 (1992); Nucl. Phys. B **392**, 461 (1993) [arXiv:hep-ph/9206229].
- [28] B. Hartmann and J. Urrestilla, J. Phys. Conf. Ser. **229** (2010) 012008 [arXiv:0911.3062 [gr-qc]].
- [29] P. M. Saffin, JHEP **0509**, 011 (2005) [arXiv:hep-th/0506138].
- [30] B. Hartmann and J. Urrestilla, JHEP **0807** (2008) 006 [arXiv:0805.4729 [hep-th]].